The Eastern Subtropical Pacific Origin of the Equatorial Cold Bias in Climate Models: A Lagrangian Perspective

MATTHEW D. THOMAS AND ALEXEY V. FEDOROV

Department of Geology and Geophysics, Yale University, New Haven, Connecticut

(Manuscript received 16 November 2016, in final form 17 March 2017)

ABSTRACT

Global climate models frequently exhibit cold biases in tropical sea surface temperature (SST) in the central and eastern equatorial Pacific. Here, Lagrangian particle back trajectories are used to investigate the source regions of the water that upwells along the equator in the IPSL climate model to test and confirm the hypothesis that the SST biases are caused by remote biases advected in from the extratropics and to identify the dominant source regions. Water in the model is found to be sourced primarily from localized regions along the western and eastern flanks of the subtropical gyres. However, while the model SST bias is especially large in the northwestern subtropical Pacific (about −5°C), it is found that the eastern subtropics contribute to the equatorial bias the most. This is due to two distinct subsurface pathways connecting these regions to the equator. The first pathway, originating in the northwestern subtropical Pacific, has relatively long advection time scales close to or exceeding 60 yr, wherein particles recirculate around the subtropical gyres while descending to approximately 500 m before then shoaling toward the equatorial undercurrent. The second pathway, from the eastern subtropics, has time scales close to 10 yr, with particles following a shallow and more direct route to the equator within the upper 200 m. The deeper and longer pathway taken by the western subtropical water ensures that vertical mixing can erode the bias. Ultimately, it is estimated that relatively confined regions in the eastern subtropics of both hemispheres control approximately half of the equatorial bias.

1. Introduction

A cold sea surface temperature (SST) bias in the cold tongue and its extension along the equatorial band of the Pacific Ocean is a consistent and recurrent feature of climate general circulation models (GCMs), including those from phase 5 of the Coupled Model Intercomparison Project (CMIP5) (Lin 2007; Li et al. 2015). The equatorial cold tongue in these models is typically too cold by about 2°C in comparison to observations and reaches too far west (Burls et al. 2017). This has significant implications for the accuracy of climate model simulations, given the strong coupling of tropical Pacific SSTs to atmospheric circulation (e.g., Pan and Oort 1983; Alexander et al. 2002; Li and Xie 2014). Gaining a full understanding of the causes of the bias has been difficult, owing to the coupled nature of tropical ocean–atmosphere dynamics that makes it complicated to isolate cause and effect in complex models. Here we apply a Lagrangian back trajectory analysis to the ocean component of one of the CMIP5 models (IPSL-CM5A-MR) to identify the remote source regions of water for the equatorial Pacific and directly assess their relative contributions to the cold tongue bias.

Recent studies have now demonstrated a consistent relationship in models between the equatorial SST bias and remote extratropical SST biases, specifically in the subtropical gyre regions (Vannière et al. 2014; Burls and Fedorov 2014). In CMIP5 these remote biases are suggested to arise as a result of deficiencies in surface shortwave fluxes and then propagate to the cold tongue (Burls et al. 2017). It remains unclear, however, which remote regions have a dominant control on the equatorial temperature bias and whether the anomalies are advected to the equatorial Pacific or radiated by waves (Vannière et al. 2014).

The cold tongue is a zonally oriented band of relatively cold water located in the central and eastern equatorial Pacific (for brevity, we will refer to this region as EEP). It arises as a consequence of Ekman divergence along the equator, which upwells deeper water to the surface that then spreads westward under the

Corresponding author: Matthew D. Thomas, matthew.thomas@yale.edu

DOI: 10.1175/JCLI-D-16-0819.1

action of easterly winds. The southeastern extension of the cold tongue, along the west coast of South America, is controlled by other processes (e.g., Takahashi and Battisti 2007) and is not considered here. The upwelling water in the cold tongue originates primarily from the subtropical gyre regions, where it subducts from the ocean mixed layer before then flowing toward the equator in the subsurface layers of the shallow wind-driven subtropical cells (STCs) (e.g., McCreary and Lu 1994; Liu and Huang 1997; Gu and Philander 1997; Harper 2000; Izumo et al. 2002; Rodgers et al. 2003). It finally reaches the surface EEP via the Equatorial Undercurrent (EUC). Previous studies have demonstrated that persistent changes in the source temperature of this water modify the temperature of the cold tongue (e.g., Boccaletti et al. 2004; Fedorov et al. 2004, 2007; Yu and Sun 2009; Vannière et al. 2014; Burls et al. 2017). Theories of tropical ocean adjustment indicate that the ocean response to such extratropical forcing involves Rossby and Kelvin wave propagation, advection by mean currents, and diabatic effects modifying net ocean heat content. Which effects dominate depends on the relevant time scales, geographic location of the forcing, and other factors (Johnson and Marshall 2002; Boccaletti et al. 2004; Fedorov et al. 2004, 2007).

Burls et al. (2017) have suggested that the advective pathway of the STCs explains the connection between the SST biases of the extratropics and EEP, which they found to hold in the CMIP5 models as well as in experiments with modified extratropical albedo using the Community Earth System Model (CESM). Vannière et al. (2014) have also demonstrated that the cold tongue bias takes about 30 years to develop in a climate model simulation in which they restored SSTs to observations before allowing the model to return to equilibrium. Such a relatively long timeframe suggests that the biases are advected in from a nonlocal source. In their analysis they showed that the temperature biases can propagate from the western subtropical gyre to the EEP via the western boundary. Since the largest SST biases are typically found at the western side of the subtropical gyres in CMIP5 models, particularly in the Northern Hemisphere, the region has been considered to be the principal source of the cold tongue bias.

Other possible causes of the EEP SST bias proposed in the literature are related to errors in local equatorial processes. These include problems in the incoming radiation budget caused by poor parameterizations for clouds [and therefore albedo (Sun et al. 2003)] or convection (Song and Zhang 2009), too much upwelling that results from excessively strong trade winds (Guilyardi et al. 2009), problems in surface coupling and feedbacks (Lin 2007), erroneous mixing processes along the equator that affect equatorial upwelling (Moum et al. 2013), or problems in the representation of ocean biogeochemical attenuation of tropical surface radiation (Murtugudde et al. 2002). However, these are inconsistent with the approximately 30-yr development time scale of the EEP bias that was reported by Vannière et al. (2014), and indeed on short time scales the equatorial band first warmed in their experiment before then beginning to cool some years later. Thus, local processes may be able to amplify the bias, but appear not to be the cause of it in the first place. While Vannière et al. (2014) analyzed only one climate GCM, they demonstrated that the model biases showed many similar characteristics to those in many of the other CMIP5 models.

Another common feature of CMIP5 temperature biases is the additional presence of too-warm temperatures that underlie the surface cold biases in the subtropics, typically below 200–300-m depth (Burls et al. 2017). Such a vertical structure (from cold to warm) is consistent with possible erroneous vertical mixing of heat over a broader region of the Pacific extending to the midlatitudes or farther (Fedorov et al. 2010; Manucharyan et al. 2011; Delworth et al. 2012; Furue et al. 2015). However, excessive diapycnal mixing of heat is likely to lead to warming of the EEP, as heat transferred downward from the surface of the subtropics is brought to the cold tongue via the wind-driven cells (Fedorov et al. 2010). The vertical structure could alternatively be due to a lack of resolved eddies in current state-of-the-art climate models, which has been suggested to result in too little upward mixing of heat toward the surface (Delworth et al. 2012; Griffies et al. 2015). An increase in model horizontal resolution was found by Delworth et al. (2012) to help alleviate much of the surface cold bias in both the EEP and the subtropical gyre, though it is not clear what processes brought this about, or if improvements in the cold tongue bias were a subsequent result of improvements to the extratropical bias. An additional possibility is that the cold tongue bias results from a combination of competing or complementary erroneous processes, such as biases in both vertical mixing and subtropical surface shortwave fluxes.

Here, we investigate the extent to which the cold tongue surface temperature bias is related to remote SST biases advected into the EEP. We use a Lagrangian particle-tracking tool Ariane (Blanke and Raynaud 1997), with the IPSL-CM5A-MR, to trace the origins of water that upwells into the EEP and then compare their endpoint properties. This method allows us to directly test the advective link between SSTs of different regions, an otherwise complicated task in a circulation system composed of multiple pathways and time scales.

The work builds on earlier studies that have successfully applied Lagrangian methods to determine the origins of upwelled equatorial water (Harper 2000; Gu and Philander 1997; Izumo et al. 2002; Rodgers et al. 2003). We do not investigate the origin of the remote bias and focus only on the oceanic interconnectivity. We instead refer the reader to the comprehensive analysis of the CMIP5 models by Burls et al. (2017), who discussed model deficiencies in low clouds as a potential source of the extratropical bias.

In section 2 we describe the model and Lagrangian tools that we have used in this analysis. The results are then described in section 3, in which we first look at the origins of water that upwells into the EEP (the last place it left the mixed layer) before identifying the relationship between the temperature biases of the subtropics and the cold tongue and finally tracing the advective pathways out of the subtropical Pacific. A discussion and conclusions of the results are provided in section 4.

2. Numerical tools

a. Model description

The model used in this study is the IPSL-CM5A-MR (Dufresne et al. 2013), which contributed to CMIP5 (Taylor et al. 2012). It is a model similar to the one used by Vannière et al. (2014), but with a higher atmospheric resolution. The ocean component of this model employs NEMO, version 3.2 (Madec 2008), with ORCA2 grid configuration (Madec and Imbard 1996), which has a nominal 2° horizontal resolution and 31 unevenly spaced vertical layers that increase in thickness with depth. The latitudinal resolution is refined to 0.5° in the tropics. A partial step configuration is used to better resolve the bathymetry (Barnier et al. 2006). It has a tripolar global grid that becomes a Mercator grid equatorward of 40° latitude, which is the region of principal interest in this study. Parameterizations include a turbulent kinetic energy mixed layer scheme (Blanke and Delecluse 1993) and the Gent and McWilliams (1990) eddy parameterization that is reduced in the tropics and zero at the equator. The eddy-induced velocities from the Gent and McWilliams (1990) parameterization are included as part of the total velocity used to advect the Lagrangian particles. Horizontal eddy viscosity and lateral eddy diffusivity are 4×10^4 and $10^3\,m^2\,s^{-1}$, respectively, except in the tropical interior ocean where they are both equal to the latter. The ocean model is coupled to the sea ice model Louvain-la-Neuve Ice Model, version 2 (LIM2) (Fichefet and Maqueda 1997), the land model ORCHIDEE (Lathiere et al. 2005), the atmospheric model LMDZ (Tiedtke 1989), and the biogeochemical

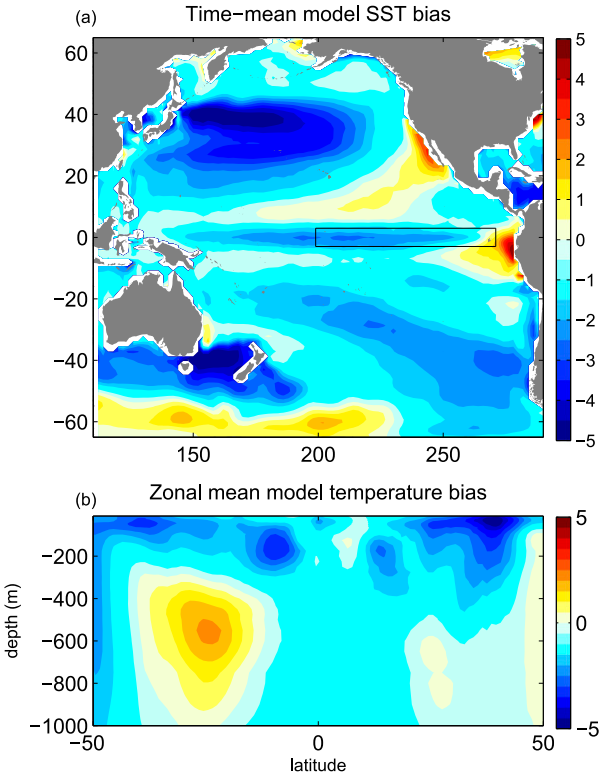

FIG. 1. Model bias (°C) in (a) SST and (b) zonal-averaged temperature as a function of depth for the Pacific Ocean. Biases are calculated oceanic mean fields from the IPSL-CM5A-MR minus the 1870–1920 SSTs from HadISST in (a) and *WOA13* temperatures in (b). The black box delineates the seeding region for the Lagrangian experiments.

model Pelagic Interaction Scheme for Carbon and Ecosystem Studies (PISCES) (Aumont and Bopp 2006). (Expansions of acronyms are online at http://www.ametsoc.org/PubsAcronymList.) Spinup for the physical components of the climate model exceeded 4000 yr. Here, we analyze ocean output from a preindustrial control configuration of the model with 1900 yr of monthly data. For more details on the components and spinup of the model, the reader is referred to Dufresne et al. (2013).

Similar to other CMIP5 models (Burls et al. 2017), the IPSL model exhibits a time-mean surface cold bias along the equatorial band (Fig. 1a), which is calculated here as the model SST minus climatological monthly observations of the period 1870–1920 from the HadISST sea surface temperature database (Rayner et al. 2003). The SST bias in the EEP, averaged within 3° of the equator and over the full time period, is about −2°C. There is also a strong subtropical cold bias, particularly at the western sides of the gyres. Calculation of the zonal mean temperature bias with depth shows that surface subtropical biases translate downward and equatorward away from the surface into the

subsurface ocean. A deep warm bias is present in the model below this (Fig. 1b), calculated as the zonal average of the model temperatures minus those from the *World Ocean Atlas 2013* (*WOA13*) database (Locarnini et al. 2013). This bias mostly appears in the interior ocean away from the western boundary (not shown). It is unclear what causes the warm bias, which may be the result of too much downward mixing of heat from the surface or a lack of eddy-induced upward mixing of heat (Delworth et al. 2012; Griffies et al. 2015), but it is a common feature of the CMIP5 models (Burls et al. 2017). Surface warm biases along the coasts of Mexico and Peru are also common to other models and are usually explained as being caused either by insufficient stratus cloud cover and/or weak coastal upwelling (e.g., Mechoso et al. 1995; Richter 2015). The temperature biases in the IPSL model have been shown to have many similar characteristics to those produced in the other CMIP5 models (Vannière et al. 2014; Burls et al. 2017), suggesting that the results presented here are relevant also to those models.

b. *Lagrangian tool and experiments*

The Lagrangian ocean analysis tool Ariane (Blanke and Raynaud 1997; see http://www.univ-brest.fr/lpo/ariane) is applied in this study to determine the remote origins and properties of EEP upwelling water. Ariane can be used to seed particles onto the grid of a numerical model and then integrate their positions back in time according to the output velocity fields of the model. The particles therefore trace water mass trajectories according to the terms in the momentum equation. Throughout the paper we do not distinguish between advection of mass and heat, which is equivalent to neglecting tracer diffusion in the heat equation: as we discuss later, scaling arguments suggest this term will be small for our purposes.

Particles can be seeded at any location or time in the model, and can be traced until they satisfy some chosen criteria, such as when they intercept a selected control cross section or when they satisfy some Boolean argument that accounts for their position, age, or other properties. One of the principal functionalities of Ariane for our purposes is that it assigns particles a volume transport that is conserved in time. This makes it possible to quantitatively account for all of the transport through a cross section or surface and then determine its interconnectivity with other regions of the ocean.

Particles at any given place are seeded one per grid cell face at each model time step unless the transport across the cell face exceeds a user-defined particle-transport threshold. In this case the cell face and its transport is linearly divided into four in the two spatial dimensions and into two in the time dimension. Particles are then seeded one per divided grid cell unless they still exceed the threshold, whereby the process is repeated until the constraint is satisfied. The purpose of such a threshold is to allow more particles to be seeded into the model, which can therefore better sample the velocity fields. In our case, the maximum transport has been set at 0.1 Sv ($1\,\mathrm{Sv} \equiv 10^6\,\mathrm{m^3\,s^{-1}}$), but our results are not sensitive to this choice or, accordingly, to the number of seeded particles. The reader is referred to section 2c of Blanke et al. (1999) for more details of the cell subdivision.

Since the particles are integrated in time using the model monthly averaged output, an error will be incurred according to averaging of the nonlinear terms in the momentum equation. The sensitivity to this assumption was investigated using a 2° resolution ocean model similar to that used here by Valdivieso Da Costa and Blanke (2004) to test the extent to which pathways using monthly output fields deviated from those using 15-hourly output. Deviations of the individual trajectories were found to be about 8% of the distance traveled. Given the very low sensitivity of our results to changes in the number of seeded particles, we assume that the monthly averaging is not an important source of error to our results.

Positions and properties of the particles can be output either at every integration time step (the so-called qualitative mode) or at the endpoint positions only (the quantitative mode). In the latter, statistics can be compiled that provide information on the interconnectivity between different locations. As a result of the large amount of output involved in a qualitative experiment, we have mostly adopted the quantitative functionality (unless stated otherwise), as it allows us to seed a large number of particles.

We have run particles in a Pacific domain that is laterally bound by full-depth control sections located at the Bering Strait, along 55°S, along 125°E, and across the Indonesian Throughflow to the north of Australia. The domain is also vertically bound below the time-dependent mixed layer (Rodgers et al. 2003; Thomas et al. 2015), which is defined as the depth cell where the density exceeds the surface density by $0.01\,\mathrm{kg\,m^{-3}}$. This is the same threshold as has been used in other studies with models of similar resolution (e.g., Blanke et al. 2002; Rodgers et al. 2003; Thomas et al. 2015), and inspection of the subtropical density profiles reveals that indeed this depth lies consistently at or shortly below the mixed layer depth. Further, sensitivity experiments using density differences of 0.007, 0.015, and $0.03\,\mathrm{kg\,m^{-3}}$ show that our conclusions are not sensitive to the definition.

In all but one experiment (as stated below and discussed further in the results section), we have seeded particles at the base of the mixed layer in the EEP region, defined within 3°N–3°S, 160°–85°W (the black box in Fig. 1a). We then integrated their trajectories backward in time either until their point of last subduction from the mixed layer or until they intercepted one of the other domain boundaries (the vast majority of the trajectories ended at the base of the mixed layer). Although the cold bias extends farther to the west of the EEP box, we seed this region because this is where the upwelling takes place (as can be seen later in Fig. 6b). The westward extension is likely because of advection of the bias in the surface layer. Particles were seeded so that all water that obducted into the base of the mixed layer in the EEP region was accounted for at every model time step. They were seeded over a 100-yr period, located toward the end of the model run, and back traced for a maximum of 300 yr. This approach resulted in an average of approximately 1700 particles per monthly time step and over 2×10^6 seeded particles in total. The EEP obduction at each seeding location was calculated according to

$$S = -\frac{\partial h}{\partial t} - \mathbf{u}_b \cdot \nabla h - w_b, \tag{1}$$

from which only negative values of S (i.e., obduction) were retained. In Eq. (1), h is the depth of the mixed layer, and $\mathbf{u}_b$ and w_b are the horizontal and vertical velocities at the base of the mixed layer, respectively (Marshall et al. 1993; Valdivieso Da Costa et al. 2005). The mass transport into the mixed layer that results from an increase in the mixed layer depth from one time step to another [i.e., the first term on the RHS of Eq. (1)] was seeded according to the method of Blanke et al. (2002): the minimum number of particles that satisfied the particle-transport threshold was allocated and distributed evenly throughout the obducted volume. By seeding in this manner we have been able to fully account for all of the transport into the EEP mixed layer. We note that our results are similar if a simpler methodology is employed in which all particles are instead seeded in the EEP region at, for example, 50 m.

With the assumption that mixed layer temperatures are vertically homogeneous, particle SSTs can be compared to the HadISST surface climatology to determine their associated biases at each endpoint of a trajectory. This assumption of vertical homogeneity does not affect our results. While the mixed layer is generally not well defined in the EEP region because of strong stratification, it is convenient to retain a single consistent definition of the working domain. We note that the EEP bias is more easily compared to other surface temperature biases (i.e., at the same depth) than to subsurface temperature biases, so we restrict our Lagrangian analysis of the bias to mixed layer endpoint comparisons only. This is because subsurface biases are sensitive to a particle's depth, such that an additional bias can be introduced along the subsurface trajectory as a result of a particle following erroneous model circulation pathways relative to real ocean pathways. This could give the appearance that an initial surface bias is not conserved into the deeper model layers even if it is.

In one experiment that required seeding over a very long time period, as described in section 3b, we instead seeded all of the particles at 50-m depth rather than along the exact base of the mixed layer. This is because it removes the need to seed particles according to the first two terms on the RHS of Eq. (1), which otherwise more than doubles the number of required particles. The mixed layer definition outside of the EEP in this experiment was the same as in the other experiments, and test experiments demonstrate that the results are not sensitive to this change (not shown). In all experiments, we have removed particles that obducted into the EEP within 1 yr of subduction. This is done in order to remove water that subducts and obducts within a single seasonal cycle, which removes approximately 40% of the particles. Our conclusions are not affected by this removal since particle temperatures do not change much over this short period.

3. Results

a. *Remote origins of the EEP upwelled water*

In this section we use the Lagrangian particles to first identify the surface mixed layer regions that source water to the EEP and then describe the seasonality of the particles' subduction. Particles have been seeded along the base of the mixed layer at every month and traced backward in time up to their points of last subduction from the mixed layer.

The EEP particle mixed layer origins are shown as a mapped probability density function (pdf) in Fig. 2. To account for the different volume transports carried by each particle, the pdf is calculated as $\sum_{i=1}^{N} V_i / \sum_{i=1}^{M} V_i$, where i is the particle identifier, N is the number of particles that subducted from the mixed layer of each cell of a regular 2° grid, M is the total number of particles subducted from the mixed layer of the full domain, and V_i is the particle volume transport. The principal source regions are heterogeneously distributed mostly away from the equatorial band and are dominated by localized areas of the eastern and western subtropical gyres.

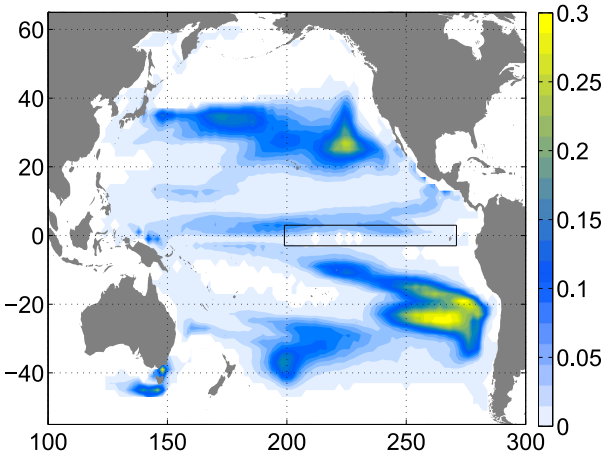

FIG. 2. Probability density function showing the origins of upwelled EEP water in the model. Particles are initialized at the base of the mixed layer in the EEP region (the Niño-3 region, shown by the black box) and run backward in time until the particles cross back into the mixed layer (mainly outside of the equatorial band). Particles have been binned onto a regular 2° × 2° grid. Units are percentage per grid cell. Spatially integrating this function would yield 100%. Note the two regions on both sides of the equator (in the western and eastern subtropical Pacific) that supply most of the waters to the equatorial cold tongue. White areas mark the regions with no communication to the EEP. All particles with a lifetime of less than 1 yr have been removed.

The origins are restricted to the subtropical gyre regions where downward Ekman pumping occurs, with a sharp cutoff at about 40° latitude that is consistent with where the wind stress curl changes sign. As we describe in more detail in section 3c, the subsurface particle pathways are limited to the wind-driven subtropical cells in the upper 600 m. The results are qualitatively consistent with earlier studies using Lagrangian particles in coarse-resolution models (Gu and Philander 1997; Harper 2000; Izumo et al. 2002; Rodgers et al. 2003) and an eddy-permitting resolution model (Goodman et al. 2005), although by having seeded and traced all of the volume transport that obducts into the mixed layer of the EEP, we can map the source locations more quantitatively.

The largest proportion of water arrives to the EEP from the Southern Hemisphere, from which the probability of a water parcel arriving to the EEP is approximately 58%. This agrees quite well with both observational (Tsuchiya et al. 1989; Rodgers et al. 1999) and higher-resolution modeling (Goodman et al. 2005; Grenier et al. 2011; Qin et al. 2015) studies that suggest about two-thirds of the water arriving to the equatorial band is sourced from the Southern Hemisphere. This is slightly more than the 58% found here, though the hydrographic observations of Tsuchiya et al. (1989) do suggest a lower bound of around 50%. Any model biases in the partitioning of source waters between the northern and Southern Hemisphere could be an alternative origin of the EEP bias. This is because a temperature gradient exists between the extratropics of the Southern and Northern Hemisphere (Rodgers et al. 1999), which in our model is approximately 1.3°C when averaged over all particle temperatures at their points of subduction. However, assuming particles retain this temperature difference on arrival into the EEP, such a contribution would only equal a small fraction of this interhemispheric temperature difference, roughly 1.3°C multiplied by the fractional error in the contribution of water from each hemisphere (of up to about 10%).

The principal source regions shown in Fig. 2 are areas with large net mixed layer subduction, as shown in earlier studies (see, e.g., Qiu and Huang 1995; Harper 2000; Liu and Huang 2012) and found also in the model used here (not shown). However, unlike the regions that source most water to the EEP, the net mixed layer subduction is largest at the western side of the Northern Hemisphere subtropical gyre. The reason for this is that winter–spring mixed layers are typically deepest here (Toyama et al. 2015). When deep winter mixed layers shoal in early spring, a large volume of water is subducted and transferred into the main thermocline by the currents, a process described by Stommel's "demon" theory (Stommel 1979; Marshall et al. 1993; Qiu and Huang 1995; Williams et al. 1995). Maps of the time-mean mixed layer depth of the particles at the time of mixed layer subduction (Fig. 3b) and their most common (modal mean) month of subduction (Fig. 3a) demonstrate that typical subtropical subduction mechanisms are responsible for sourcing water to the EEP and therefore suggest that the source regions and properties in other models could be ascertained by a simple inspection of the model springtime mixed layers. The relatively large contribution to the EEP from the eastern side of the Southern Hemisphere gyre is consistent with the "exchange windows" mechanism (Liu et al. 1994), and is a consequence of the wider extent of the South Pacific (Harper 2000). This will be discussed in more detail in section 3c.

It is noteworthy that the coldest model SST bias, located approximately between 35° and 40° latitude in both hemispheres (Fig. 1), is experienced by the particles only marginally, as there is little subduction in this region (Fig. 2).

b. Subtropical control of the tropical SST bias

We now investigate the particle temperature biases at their subduction and obduction locations and determine how well they are related. We then identify the areas that most strongly contribute to the cold tongue bias. By

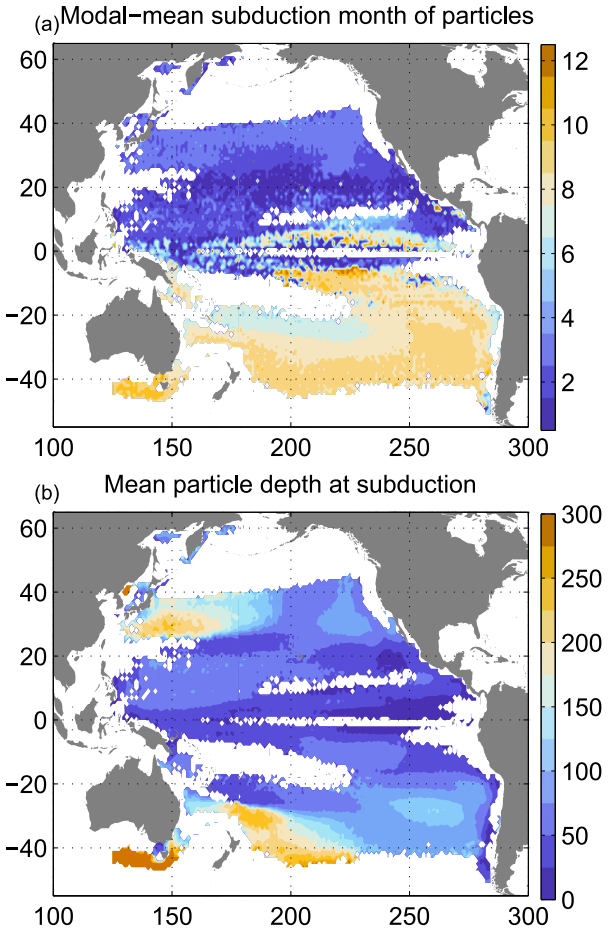

FIG. 3. (a) The most common (modal mean) month of subduction of the particles from the mixed layer, from January (1) through December (12) and (b) the average depth (m) of the particles at the time of subduction. Particle positions have been binned onto a regular 2° × 2° grid.

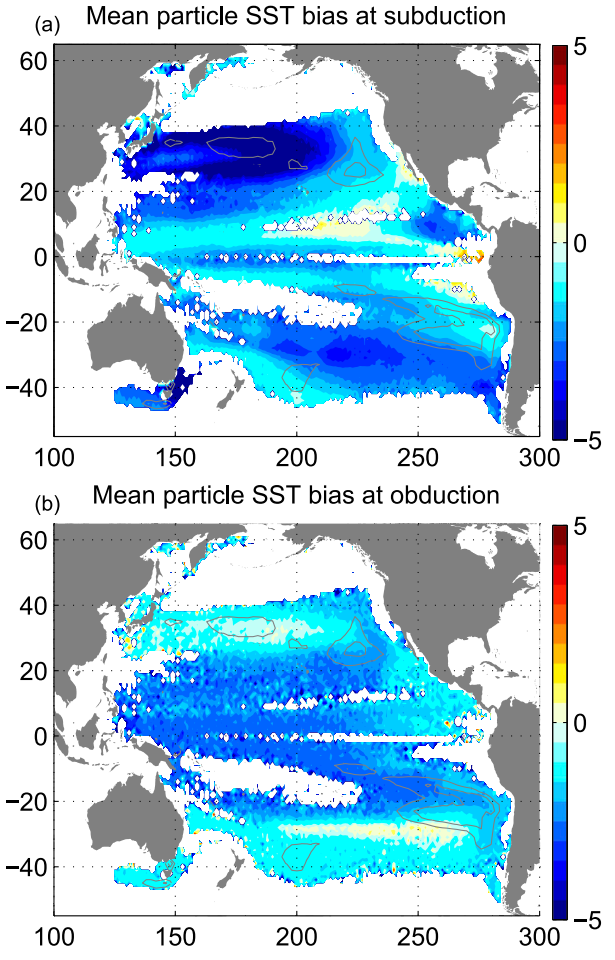

FIG. 4. Mean temperature biases (°C) of the parcels at the time of (a) subduction in the extratropics and (b) obduction into the EEP mixed layer, mapped onto their locations at the time of subduction. Particle positions have been binned onto a regular 2° × 2° grid. Temperature comparisons are made to surface observations under the assumption that water temperatures are uniform within the mixed layer definition used here. Note the loss of the initial bias for particles subducted inside the subtropical gyres by the time they reach the EEP. The gray lines follow the 0.1% and 0.2% contours from the water-origins pdf of Fig. 2 and indicate the main regions of subduction.

making the assumption that the mixed layer is vertically homogeneous, particle temperatures at the location and month of subduction and obduction from the mixed layer can be compared to the monthly SST climatology to determine their individual SST bias (δSST). Figure 4 shows such maps of the average particle δSST, at the points of subduction and obduction, calculated as a transport-weighted average in each cell of a regular 2° grid according to

$$\overline{\delta\mathrm{SST}} = \frac{\sum_{i=1}^{N} V_i \delta\mathrm{SST}_i}{\sum_{i=1}^{N} V_i}, \qquad (2)$$

where the overbar represents an average.

The distribution of $\overline{\delta\mathrm{SST}}$ at the point of last subduction from the mixed layer (Fig. 4a) is broadly similar to the model full time-mean SST bias (Fig. 1a), but with some key exceptions related to the seasonality and spatial restrictions of particle subduction: particles arrive from limited regions of the tropics and subtropics, thereby excluding some regions with the coldest temperature biases in the Pacific; the particle $\overline{\delta\mathrm{SST}}$ values in the eastern subtropics are colder than the model time-mean biases; particle $\overline{\delta\mathrm{SST}}$ values are colder in the eastern North Pacific to the south of 10°N; and particle $\overline{\delta\mathrm{SST}}$ values are colder in regions of the western subtropical gyres. Given the dominant springtime subduction of the particles (Fig. 3b), this demonstrates that

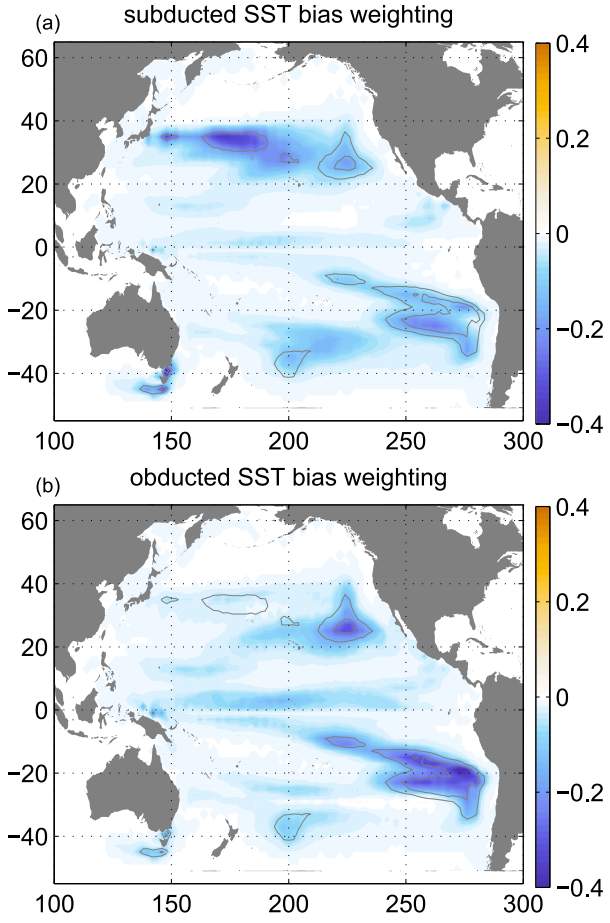

FIG. 5. Probability density function showing the origins of upwelled EEP water, as in Fig. 2, but weighted by SST biases at the time of (a) subduction in the extratropics and (b) obduction into the EEP mixed layer. The black box is the EEP region from which particles are seeded at the base of the mixed layer. Units are percentage per grid cell. The pdf in (b) points to the greater importance of the eastern subtropical region for the bias. The gray lines follow the 0.1% and 0.2% contours from the water-origins pdf of Fig. 2 and indicate the main regions of subduction.

spring SST biases are often colder than the time-mean ones [see also Wang et al. (2014)], and indeed they would compare more closely with a calculation of the springtime model SST biases (calculated as March in the Northern Hemisphere and October in the Southern Hemisphere; not shown).

The mean δSST from all of the particles at their points of mixed layer subduction [determined by using the total number of particles, M instead of N in Eq. (2)] is -2.27°C. While this is a similar temperature bias to that of the cold tongue itself, we show below that it is unlikely that all of this temperature bias is preserved along the pathways to the EEP.

If we weight the pdf of the source waters (Fig. 2) by the particle δSST values at the point of subduction (Fig. 4a), then we can assess the relative importance of the different regions for the cold tongue bias under the assumption that the particle pathways are adiabatic. This is calculated as $\sum_{i=1}^{N} V_i \delta\mathrm{SST}_i / \sum_{i=1}^{M} V_i \delta\mathrm{SST}_i$ (Fig. 5a). Such a map would suggest that the western subtropics dominate the cold tongue bias, particularly in the Northern Hemisphere, where SST biases are largest, which is the conclusion that Vannière et al. (2014) arrived at. However, if instead we use Eq. (2) to map the particle δSST values at the point of obduction into the EEP back onto their point of last subduction, then we find that the SST biases of the western subtropical gyres are lost by the time the water arrives into the EEP, while those on the eastern side of the gyre appear to be the most closely preserved of the major source regions (Fig. 4b).

This loss of the western subtropical particle $\overline{\delta\mathrm{SST}}$ values demonstrates that the subsurface pathways from here are not fully adiabatic. Furthermore, the $\overline{\delta\mathrm{SST}}$ values of particles arriving from the rest of the subtropical and tropical Pacific are similar upon arriving into the EEP, which suggests that some mixing of the temperature biases takes place. This provides further evidence that temperatures are not conserved along the subsurface pathways. But it should be noted that the $\overline{\delta\mathrm{SST}}$ values from regions that source less water to the EEP are more easily changed between subduction and obduction.

Information on where these diabatic processes occur can be explored by mapping the along-track particle temperature rates of change dT/dt calculated using the qualitative output from a random subset of 40 000 particles (Fig. 6a). The value for dT/dt is computed as the change of temperature between every two adjacent output positions along the pathways of each trajectory divided by their time difference. These values, located at the midpoint between each pair of along-track positions, are then geographically binned onto a regular 2° grid and averaged at each grid location. A map of vertical velocity, calculated as dz/dt, is calculated in a similar manner and will be discussed in the next subsection (Fig. 6b). Figure 6a shows that the particles undergo the largest temperature changes in the EEP region, where the particles warm, and also in the midlatitude western boundary currents, where the particles typically cool [see Spall (1992), who also found similar western boundary particle cooling in the Atlantic]. Aside from some warming on the eastern limbs of the subtropical gyres, the warming upon upwelling into the equatorial band accounts for much of the approximately 5°C temperature change from the subtropics to the EEP. This strong warming is largely controlled by a balance between vertical and horizontal advection and vertical

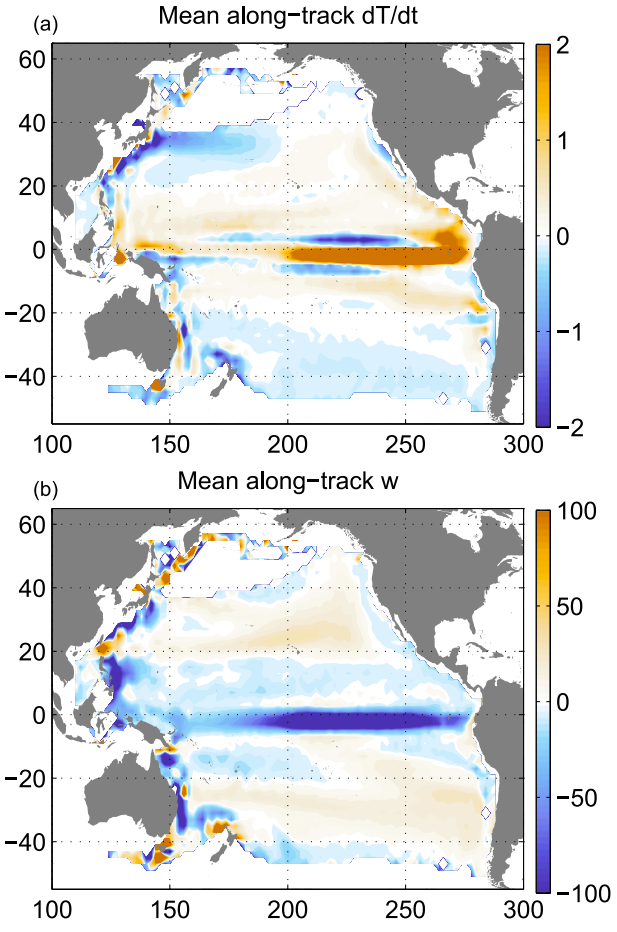

FIG. 6. Average (a) dT/dt (°C yr^{-1}) and (b) w (m yr^{-1}; calculated as dz/dt) of particles, along the particle tracks (see text). A random subset of 40 000 particles was used. All particle properties have been binned onto their geographical position on a regular 2° grid and then averaged at each location. Positions of both dT/dt and w are calculated at the midpoint of two adjacent positions along a particle trajectory.

mixing (Yin and Sarachik 1993), which is parameterized according to the turbulent kinetic energy (TKE) closure scheme (Blanke and Delecluse 1993; Madec 2008).

Although the subsurface pathways are not adiabatic, this does not mean that the temperature biases are not conserved. They would be conserved if the diabatic processes are well represented by the model. SST biases from the eastern subtropics appear from Fig. 4 to be approximately conserved, though it is possible that they change a lot in the subsurface before then changing back. Next, we will test whether remote particle biases are related to EEP biases by comparing 1800-yr time series of the spatially averaged particle δSST values at the points of subduction and the full EEP SST bias (calculated directly from the model output and not using particles, although we note that it closely matches the time series of the particle SST bias at the points of obduction). Sufficiently long temporal deviations in the extratropical biases, if conserved along the subsurface pathways to the EEP, should occur in both time series. Such a comparison of the EEP bias to only the endpoints of the trajectories allows us to directly compare them without the need to lag adjust the two time series.

As described in section 2b, to create the long time series we have seeded all of the particles in the EEP region at 50-m depth in order to reduce computing requirements. Particles were seeded every month of the 1800-yr time series, and each particle was traced for 100 yr. The particles were then binned into 4-yr averages so as to ensure that a representative number of particles is accounted for at each discrete time step and also to avoid sampling the seasonal cycle. To test the extent to which the extratropical particles can account for the EEP bias, we have filtered out of the subduction time series all particles whose mixed layer origins are within 10° latitude of the equator. The EEP bias is also binned into 4-yr averages. We are interested in the quasi-steady-state time scales of the cold tongue bias and, therefore, low-pass filter both time series at a cutoff period of 60 yr. This is long enough to ensure that the dominant advection time scales between the subtropics and the EEP have been exceeded.

The time series of the subduction and EEP biases have a correlation coefficient at zero lag of approximately 0.62 (Fig. 7), which is significant at the 95% threshold according to a block bootstrap calculation of significance [see appendix D of Thomas (2012) for details of the method]. The mechanism of variations in these two time series, with a period of about 90–100 yr, is likely to be related to the mechanism proposed by Gu and Philander (1997), in which the extratropics and the equatorial cold tongue are linked by the oceanic bridge as well as weak ocean–atmospheric coupling. Overall, the agreement between the two time series is impressive given the broad range of pathways, time scales, and seasonality that make up the time series, as well as the large number of processes that affect the particles.

We now further filter the time series to test the conclusion that eastern subtropical biases are responsible for the EEP bias. The subduction time series are filtered so as to only include particles that subducted from specific subregions of the Pacific subtropical gyres (Fig. 7). We apply this filter for four different subregions of the subtropics: the northeastern Pacific, southeastern Pacific, northwestern Pacific, and southwestern Pacific (the boundaries of which are delineated in Fig. 9). The correlation coefficients with the EEP obduction time series for these subregions are 0.29, 0.56, −0.02, and 0.08, respectively. Both of the correlations for the eastern side

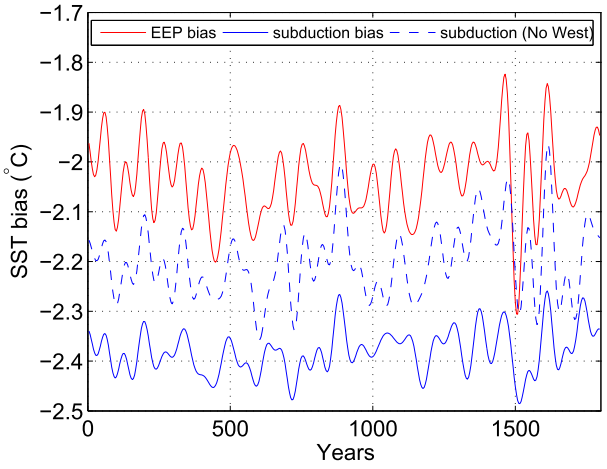

FIG. 7. Time series of the average model SST bias (°C) in the EEP region (red) and the spatial-mean SST biases of the particles at their extratropical points of subduction (blue), which correlate to a value of 0.62. If particles that subducted from the western subtropical regions are removed, then the correlation is 0.67 (blue dashed; for presentation purposes this curve has been offset by −0.6°C; see text for details). When computing the subduction time series, the particles are binned and averaged into time increments of 4 yr; all time series are then low-pass filtered at a cutoff of 60 yr. The time axis refers to the EEP SST bias. To save on computing resources, all particles have been seeded at 50 m in the EEP region (black box in Fig. 1) instead of at the base of the mixed layer.

of the basin are significant at 95%. The proportions are what we would expect considering both the relative contributions of water provided to the EEP from those regions (Fig. 2) and the extent to which the $\overline{\delta SST}$ values from the regions change between subduction and obduction (Fig. 4). Since the western subtropical particles are not correlated to the EEP bias, the 0.62 correlation between the EEP bias and the full extratropical subduction bias, as reported above, is increased to 0.67 if the particles from the western subtropics are filtered from it. Furthermore, the resulting time series also then displays very similar-magnitude variability to that of the EEP bias time series, which otherwise displayed weaker variability.

We note that similar results are produced if the correlation analysis is instead done using SST anomaly (calculated relative to the time-mean monthly temperature climatology of the model) rather than SST bias–significant correlations are found when correlating the EEP anomalies to those of the eastern subtropical regions, but not to those of the western regions.

With the direct evidence that the extratropics impact the EEP bias remotely, we can now quantify the relative importance of the different source regions by weighting the particle origins pdf of Fig. 2 by the final obducted particle δSST values of Fig. 4b, as is shown in Fig. 5b. The eastern subtropical gyres have the greatest impact on the EEP bias, with the two localized regions of the Pacific making up approximately 50% ± 5% of the total remote contribution (calculated as a sum of the relevant areas in Fig. 5b). These are regions which are known to have too-weak net incoming surface heat flux in CMIP5 models (Zuidema et al. 2016). Corrections to these fluxes in models may therefore result in a strong improvement in model climate fidelity. A calculation of the mean δSST of all particles at their point of obduction [replacing N with M in Eq. (2)] now shows that the particles contribute only −1.51°C. This is approximately 0.3°C less than the cold tongue bias, which suggests that some additional process is acting to augment this incoming cold bias contribution, such as local positive ocean–atmosphere feedbacks (e.g., Dijkstra and Neelin 1995).

The results are consistent with the conclusion that water subducted from the surface mixed layer of the subtropics has an important control on the cold tongue bias (Vannière et al. 2014; Burls and Fedorov 2014; Burls et al. 2017), but we find that water from the eastern subtropics has the largest effect. This differs with the findings of Vannière et al. (2014), who proposed that the western subtropics are the major source. This difference may be related to their methodology, which involved forcing their model out of equilibrium according to surface flux adjustments. On removal of the flux adjustments, they found that the western subtropical SST bias propagated toward the equator, but this could have been a transient response. If they had allowed enough time for the model to return to a full equilibrium, it is possible that the western subtropical bias would have had a weaker effect on the EEP.

c. *Subsurface pathways of the wind-driven overturning cells*

In this section we explore why water that leaves the mixed layer of the western subtropical gyre in the model loses its large initial temperature bias, while the bias that originates from the eastern side of the gyres does not change much. This can be understood by analyzing the lifetimes and pathways taken by the particles, which reveal that there are two very distinct routes out of the subtropics.

Figure 8a shows the average particle age at the time of obduction into the EEP [calculated as in Eq. (2), but replacing δSST with particle age], mapped back onto the subduction locations. Particles that subduct from the mixed layer of the western subtropics take much longer than those from the eastern subtropics, on the order of 60 versus 10 yr, respectively. Closer to the equator in the tropical belt, average travel times in the model are

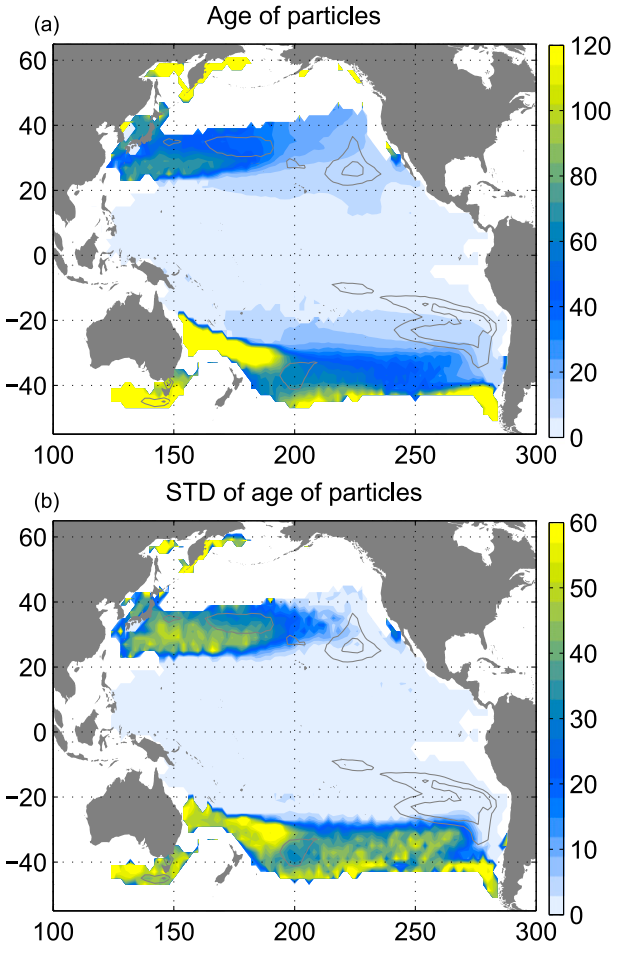

FIG. 8. (a) Mean and (b) standard deviation of the particle ages (yr) mapped onto the particles' locations at time of subduction. Particles have been binned onto a regular 2° × 2° grid. A particle's age is defined as the time span between the particles subduction and obduction events. The gray lines follow the 0.1% and 0.2% contours from the water-origins pdf of Fig. 2 and indicate the main regions of subduction.

typically about 5 yr or less. These time scales compare qualitatively well with observed tracers in the EUC (Warner et al. 1996). The large differences in particle age suggest that there are different pathways out of the subtropical gyre that depend on particle position and indicate that the larger advection times from the western Pacific to the EEP may allow for more mixing and a greater loss of the initial temperature bias.

To better understand the geographical dependence of particle age, we trace out the pathways of the particles that subducted from the four different subregions of the Pacific subtropical gyres shown in Fig. 9. All particles that subducted from each region have been separately isolated and run in the qualitative mode, which records their along-track positions. Positional information is binned onto a regular 2° grid in the horizontal and 30-m grid in the vertical, and the percentage probability that a particle visits each grid cell has then been calculated in the horizontal plane (Figs. 9a,c,e,g) and in the vertical plane (Figs. 9b,d,f,h).

Two distinct routes are taken from the eastern and western sides of the gyres. The western particles recirculate around the gyres and reach depths of about 600 m before then shoaling toward the EEP via the western boundary and EUC. The eastern subtropical particles, however, take a more direct and shallow route without recirculating around the gyre, and those from the Northern Hemisphere often even bypass the western boundary altogether. Mean along-track vertical velocities and temperature changes (Fig. 6 and section 3b) reveal how particles in the western subtropics descend and cool as they circulate the gyre. This behavior is consistent with studies that have found subtropical gyre water to spiral downward under the action of Ekman pumping and increase in density because of mixing across the sloping isopycnals of the gyre (Spall 1992; Polton and Marshall 2003; Burkholder and Lozier 2011). Eastern subtropical particles, however, ascend and warm slightly as they travel directly toward the equator (Fig. 6).

The different pathways explain the very different travel times (Fig. 8), and the shallow and direct pathways from the eastern subtropics will ensure that erosion of the subducted SST biases is smaller than that from the western side of the gyre. It is feasible also that the western particles lose some of their initial temperature bias because of the presence of a deep warm bias in the model (Fig. 1b). We return to this in the discussion and conclusions in section 4. These pathways with different adiabatic characteristics are also consistent with the double thermocline theory of the gyres, which describes a strong isopycnal gradient in the upper layers that is well explained by the ventilated thermocline theory of Luyten et al. (1983) and a deeper thermocline that is controlled by diffusion across the sloping isopycnals of the gyre (Samelson and Vallis 1997; Vallis 2000; Polton and Marshall 2003). Our results suggest that there are geographically distinct pathways onto the two thermoclines. Our conclusions are also supported by the study of Haertel and Fedorov (2012), who considered ocean circulation in a fully adiabatic limit (zero diffusivity below the ocean mixed layer) and found that in such a regime the cold tongue obduction was dominated by waters subducted in the eastern part of the basin.

The pathways taken from the different source regions, as well as spatial asymmetries in the relative contributions of water from the different source regions, can be explained according to the so-called exchange windows (Liu et al. 1994; Harper 2000). The different exchange windows, within which a parcel of water can be located,

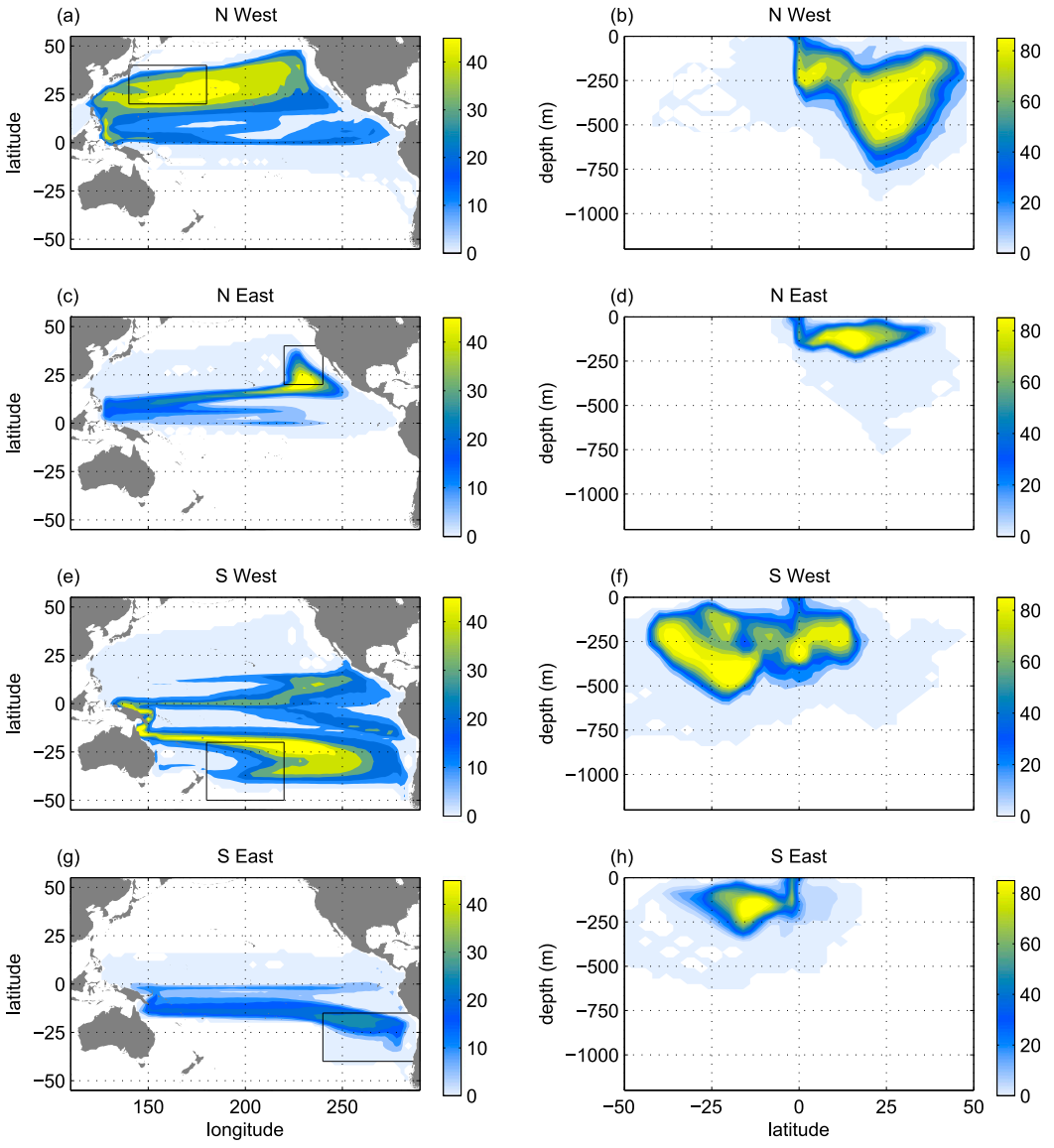

FIG. 9. Probability that particles subducting from the (a),(b) northwest; (c),(d) northeast; (e),(f) southwest; and (g),(h) southeast regions (delineated by the black boxes) will pass a particular point on the (left) latitude–longitude and (right) latitude–depth planes. Units are percentage per grid cell. In effect, these plots show the density of parcel trajectories for waters with different origins.

are delineated by longitude and determine whether a parcel of water will recirculate back around the gyre or turn toward the equator on reaching the western boundary. If a Northern Hemisphere parcel arrives at the western boundary to the north of approximately 16°N (in the Kuroshio) then it will recirculate around the gyre; if the parcel instead reaches the western boundary south of approximately 16°N (in the Mindanao Current) then it will turn equatorward. Therefore, under the assumption that all parcels flow toward the equator in roughly the same direction (e.g., southwestward in the Northern Hemisphere), the likelihood of a subtropical parcel reaching the western boundary to the south of the critical latitude is higher the farther east the particle is. Particles west of a threshold longitude are in the recirculation window, while east of it they enter the boundary exchange window. This explains why the eastern side of the gyre is the dominant regional source of water to the EEP despite net mixed layer subduction being larger at the western side of the gyre. The wider basin width in the Southern Hemisphere therefore explains why it sources most water (Harper 2000).

A couple of additional interhemispheric differences exist in the pathways. Particles subducted from the northeastern subtropical Pacific are more likely to avoid the western boundary altogether than those subducted from the south (cf., for example, the 15% contours in Figs. 9c,g). This is because the North Equatorial Countercurrent acts to deflect the water toward the east as it travels south (Rothstein et al. 1998; Harper 2000). Also, the pathways taken from the southwestern subtropical Pacific tend to stay in the interior part of the gyre without passing into the western boundary current, presumably because of interhemispheric differences in bathymetry at the depths at which the particles leave the mixed layer. On arrival at the equator these particles then tend to overshoot the equator. This is similar to what was found in a recent Lagrangian analysis of an eddy resolving model, in which recirculation features near the western side of the equator caused the particles to cross into the Northern Hemisphere before recirculating back toward the equator (Qin et al. 2015).

4. Discussion and conclusions

The presence of sea surface temperature (SST) cold biases along the equatorial Pacific poses serious problems for the ability of global climate models to accurately simulate the climate. We have analyzed Lagrangian particles, seeded at the base of the mixed layer of the ocean component of the IPSL-CM5A-MR and traced backward in time, to test and confirm that the too-cold (by about 2°C) Eastern Equatorial Pacific (EEP) SSTs are related to remote SST biases that are set in the extratropical mixed layer and subsequently advected to the equator via the wind-driven overturning cells (e.g., McCreary and Lu 1994). The subtropical source regions of water to the EEP are found to be heterogeneously distributed primarily from the eastern and western sides of the subtropical gyre (Fig. 2). Although SST biases at the western side of the gyres are larger, such that it would ensure they dominate the EEP SST bias if subsurface pathways were adiabatic, we find that subduction from the eastern side is the largest regional source of the bias (Fig. 5).

Time series of the subduction and obduction SST biases demonstrate that the two are well related at time scales longer than 60 yr, with a correlation coefficient of 0.59 (Fig. 7). This correlation is dominated by water sourced from the eastern subtropical regions. We consider the correlation to be very good, considering a large spatial, temporal, and seasonal spread in the origins of the particles that arrive into the EEP. We find close to zero correlation with the temperature of water sourced from the western subtropical regions. These correlations further confirm that the cold tongue bias is controlled to a large extent by the remote temperature biases of the eastern subtropical gyre when considered on time scales that exceed the equilibrium travel times associated with the wind-driven subtropical cells.

Reasons for why the western subtropical particles lose their temperature bias, while the eastern particles do not, can be explained by the different properties of two separate subsurface pathways toward the equator (Fig. 9). The pathway out of the western subtropics has a time scale on the order of 60 yr or more and reaches a depth of about 600 m (Figs. 8 and 9). This is because water slowly recirculates around the gyre while sinking under the action of Ekman pumping (Spall 1992; Polton and Marshall 2003; Burkholder and Lozier 2011). Pathways out of the eastern subtropics, however, do not circulate around the gyre but instead take a shallow southwestward path directly toward the western equatorial region at a depth of about 200 m. Consequently, time scales are typically shorter than 10 yr. This shallow and short-time-scale pathway therefore allows less time for water properties to be altered by mixing. The different pathways are a consequence of the exchange windows mechanism (Liu et al. 1994), which explains why a particle's likelihood of reaching the equator from the subtropical gyre is increased with distance toward the east (see section 3c for details).

The loss of temperature bias of the western subtropical water on the way to the equator may also be partly a consequence of a deeper warm bias [typical of many CMIP5 models (Burls et al. 2017)], which this water passes through and can mix with. However, we suggest that the contribution from this warm bias is likely to be small. This is because only a relatively small number of the particles experience the warm bias. Particles from the western subtropics of the Northern Hemisphere also lose their bias, yet very few of them pass through the warm bias (Figs. 1b and 9b,f). We propose instead that the biases are lost primarily as a result of the long interconnecting pathways. As such, we caution against the common assumption that the subsurface flow is fully adiabatic. At time scales on the order of 60 yr and longer, diabatic effects have to be considered.

Particle trajectories do not account for the diffusion of tracers in the model, so temperature pathways can be expected to differ somewhat from the mass transport pathways presented here. Importantly, however, velocities from the Gent and McWilliams (1990) subgrid-scale parameterization for eddy-induced tracer transports are explicitly accounted for in the momentum equation. Furthermore, scaling arguments suggest that the effect of horizontal diffusion on heat advection will be relatively small. Given a horizontal mixing coefficient of $\kappa_h = 10^3\,\mathrm{m^2\,s^{-1}}$, and a distance of 35° latitude (the approximate distance to the water source regions in the western subtropical gyre), it

would take approximately 180 yr for temperature to be diffused to the equator, which is much smaller than the advected time scales presented here. However, a Lagrangian analysis of the temperature pathways would be useful and is left for further work.

Previous studies have highlighted the importance of the subtropical gyres in setting the properties of the EEP via the wind-driven cells, and have suggested that they control the SST properties of the cold tongue in models. Our results support and refine this perspective by demonstrating how only a relatively small patch of the subtropics, on the eastern side of the basin, contributes to the equatorial biases, while the largest subtropical biases, on the western side, have little effect. The consistency of the model subduction processes (e.g., Qiu and Huang 1995), pathways (e.g., Harper 2000), and characteristics of the temperature biases (Vannière et al. 2014; Burls et al. 2017) to those presented in other modeling studies lends support to the relevance of our main conclusions to other climate models. We propose that improvements in the equatorial cold bias could be achieved by correcting known model biases in surface heat flux in the eastern subtropics, which typically cool the surface ocean too much (e.g., Zuidema et al. 2016). In the meantime, a simple correction that could significantly improve model climate fidelity might be achieved by applying a flux correction to only the eastern subtropical areas where springtime mixed layers are deep, which will be investigated in a follow-up study.

Acknowledgments. This research is supported by grants from NOAA (NA14OAR4310277) and NSF (AGS-1405272 and AGS-0163807). The authors are grateful for access to the freely available *World Ocean Atlas 2013* (online at https://www.nodc.noaa.gov/OC5/woa13/), the HadISST data (online at http://www.metoffice.gov.uk/hadobs/hadisst/), and the CMIP5 data (online at http://cmip-pcmdi.llnl.gov/cmip5/data_portal.html). To process the CMIP5 data, this study benefited from the IPSL mesocenter facility, which is supported by CNRS, UPMC, Labex L-IPSL, which is funded by the ANR (Grant ANR-10-LABX-0018), and by the European FP7 IS-ENES2 project (Grant 312979). We particularly thank Julie Deshayes and Sébastien Denvil at IPSL for providing both access and help with the model data and also Bruno Blanke, Nicolas Grima, and Mélanie Grenier for their advice and help with the Ariane Lagrangian model. We also acknowledge Natalie Burls, Les Muir, and Shineng Hu for interesting and helpful discussions. Constructive comments from three reviewers were greatly appreciated.

REFERENCES

Alexander, M. A., I. Bladé, M. Newman, J. R. Lanzante, N. C. Lau, and J. D. Scott, 2002: The atmospheric bridge: The influence of ENSO teleconnections on air–sea interaction over the global oceans. *J. Climate*, **15**, 2205–2231, doi:10.1175/1520-0442(2002)015<2205:TABTIO>2.0.CO;2.

Aumont, O., and L. Bopp, 2006: Globalizing results from ocean in situ iron fertilization studies. *Global Biogeochem. Cycles*, **20**, GB2017, doi:10.1029/2005GB002591.

Barnier, B., Y. D. Penhoat, L.-L. Fu, R. Morrow, J. Verron, and P. Woodworth, 2006: Impact of partial steps and momentum advection schemes in a global ocean circulation model at eddy-permitting resolution. *Ocean Dyn.*, **56**, 543–567, doi:10.1007/s10236-006-0082-1 .

Blanke, B., and P. Delecluse, 1993: Variability of the tropical Atlantic Ocean simulated by a general circulation model with two different mixed-layer physics. *J. Phys. Oceanogr.*, **23**, 1363–1388, doi:10.1175/1520-0485(1993)023<1363:VOTTAO>2.0.CO;2.

——, and S. Raynaud, 1997: Kinematics of the Pacific Equatorial Undercurrent: An Eulerian and Lagrangian approach from GCM results. *J. Phys. Oceanogr.*, **27**, 1038–1053, doi:10.1175/1520-0485(1997)027<1038:KOTPEU>2.0.CO;2.

——, M. Arhan, G. Madec, and S. Roche, 1999: Warm water paths in the equatorial Atlantic as diagnosed with a general circulation model. *J. Phys. Oceanogr.*, **29**, 2753–2768, doi:10.1175/1520-0485(1999)029<2753:WWPITE>2.0.CO;2.

——, S. Speich, and G. M. Madec, 2002: A global diagnostic of interior ocean ventilation. *Geophys. Res. Lett.*, **29**, 1267, doi:10.1029/2001GL013727.

Boccaletti, G., R. C. Pacanowski, S. G. H. Philander, and A. V. Fedorov, 2004: The thermal structure of the upper ocean. *J. Phys. Oceanogr.*, **34**, 888–902, doi:10.1175/1520-0485(2004)034<0888:TTSOTU>2.0.CO;2.

Burkholder, K. C., and M. S. Lozier, 2011: Subtropical to subpolar pathways in the North Atlantic: Deductions from Lagrangian trajectories. *J. Geophys. Res.*, **116**, C07017, doi:10.1029/2010JC006697.

Burls, N. J., and A. V. Fedorov, 2014: What controls the mean east–west sea surface temperature gradient in the equatorial Pacific: The role of cloud albedo. *J. Climate*, **27**, 2757–2778, doi:10.1175/JCLI-D-13-00255.1.

——, L. Muir, E. M. Vincent, and A. V. Fedorov, 2017: Extratropical origin of equatorial Pacific cold bias in climate models with links to cloud albedo. *Climate Dyn.*, doi:10.1007/s00382-016-3435-6, in press.

Delworth, T. L., and Coauthors, 2012: Simulated climate and climate change in the GFDL CM2.5 high-resolution coupled climate model. *J. Climate*, **25**, 2755–2781, doi:10.1175/JCLI-D-11-00316.1.

Dijkstra, H. A., and J. D. Neelin, 1995: Ocean–atmosphere interaction and the tropical climatology. Part II: Why the Pacific cold tongue is in the east. *J. Climate*, **8**, 1343–1359, doi:10.1175/1520-0442(1995)008<1343:OAIATT>2.0.CO;2.

Dufresne, J. L., and Coauthors, 2013: Climate change projections using the IPSL-CM5 Earth System Model: From CMIP3 to CMIP5. *Climate Dyn.*, **40**, 2123–2165, doi:10.1007/s00382-012-1636-1.

Fedorov, A. V., R. C. Pacanowski, S. G. Philander, and G. Boccaletti, 2004: The effect of salinity on the wind-driven circulation and the thermal structure of the upper ocean. *J. Phys. Oceanogr.*, **34**, 1949–1966, doi:10.1175/1520-0485(2004)034<1949:TEOSOT>2.0.CO;2.

——, M. Barreiro, G. Boccaletti, R. Pacanowski, and S. G. Philander, 2007: The freshening of surface waters in high latitudes: Effects on the thermohaline and wind-driven circulations. *J. Phys. Oceanogr.*, **37**, 896–907, doi:10.1175/JPO3033.1.

——, C. M. Brierley, and K. Emanuel, 2010: Tropical cyclones and permanent El Niño in the early Pliocene epoch. *Nature*, **463**, 1066–1070, doi:10.1038/nature08831.

Fichefet, T., and M. A. M. Maqueda, 1997: Sensitivity of a global sea ice model to the treatment of ice thermodynamics and dynamics. *J. Geophys. Res.*, **102**, 12 609–12 646, doi:10.1029/97JC00480.

Furue, R., and Coauthors, 2015: Impacts of regional mixing on the temperature structure of the equatorial Pacific Ocean. Part 1: Vertically uniform vertical diffusion. *Ocean Modell.*, **91**, 91–111, doi:10.1016/j.ocemod.2014.10.002.

Gent, P. R., and J. C. McWilliams, 1990: Isopycnal mixing in ocean circulation models. *J. Phys. Oceanogr.*, **20**, 150–155, doi:10.1175/1520-0485(1990)020<0150:IMIOCM>2.0.CO;2.

Goodman, P. J., W. Hazeleger, P. De Vries, and M. Cane, 2005: Pathways into the Pacific Equatorial Undercurrent: A trajectory analysis. *J. Phys. Oceanogr.*, **35**, 2134–2151, doi:10.1175/JPO2825.1.

Grenier, M., S. Cravatte, B. Blanke, C. Menkes, A. Koch-Larrouy, F. Durand, A. Melet, and C. Jeandel, 2011: From the western boundary currents to the Pacific Equatorial Undercurrent: Modeled pathways and water mass evolutions. *J. Geophys. Res.*, **116**, C12044, doi:10.1029/2011JC007477.

Griffies, S. M., and Coauthors, 2015: Impacts on ocean heat from transient mesoscale eddies in a hierarchy of climate models. *J. Climate*, **28**, 952–977, doi:10.1175/JCLI-D-14-00353.1.

Gu, D. F., and S. G. H. Philander, 1997: Interdecadal climate fluctuations that depend on exchanges between the tropics and extratropics. *Science*, **275**, 805–807, doi:10.1126/science.275.5301.805.

Guilyardi, E., P. Braconnot, F.-F. Jin, S. T. Kim, M. Kolasinski, T. Li, and I. Musat, 2009: Atmosphere feedbacks during ENSO in a coupled GCM with a modified atmospheric convection scheme. *J. Climate*, **22**, 5698–5718, doi:10.1175/2009JCLI2815.1.

Haertel, P., and A. V. Fedorov, 2012: The ventilated ocean. *J. Phys. Oceanogr.*, **42**, 141–164, doi:10.1175/2011JPO4590.1.

Harper, S., 2000: Thermocline ventilation and pathways of tropical–subtropical water mass exchange. *Tellus*, **52A**, 330–345, doi:10.1034/j.1600-0870.2000.d01-7.x.

Izumo, T., J. Picaut, and B. Blanke, 2002: Tropical pathways, equatorial undercurrent variability and the 1998 La Niña. *Geophys. Res. Lett.*, **29**, 2080, doi:10.1029/2002GL015073.

Johnson, H. L., and D. P. Marshall, 2002: A theory for the surface Atlantic response to thermohaline variability. *J. Phys. Oceanogr.*, **32**, 1121–1132, doi:10.1175/1520-0485(2002)032<1121:ATFTSA>2.0.CO;2.

Lathiere, J., D. A. Hauglustaine, N. De Noblet-Ducoudre, G. Krinner, and G. A. Folberth, 2005: Past and future changes in biogenic volatile organic compound emissions simulated with a global dynamic vegetation model. *Geophys. Res. Lett.*, **32**, L20818, doi:10.1029/2005GL024164.

Li, G., and S. P. Xie, 2014: Tropical biases in CMIP5 multimodel ensemble: The excessive equatorial Pacific cold tongue and double ITCZ problems. *J. Climate*, **27**, 1765–1780, doi:10.1175/JCLI-D-13-00337.1.

——, Y. Du, H. M. Xu, and B. H. Ren, 2015: An intermodel approach to identify the source of excessive equatorial Pacific cold tongue in CMIP5 models and uncertainty in observational datasets. *J. Climate*, **28**, 7630–7640, doi:10.1175/JCLI-D-15-0168.1.

Lin, J. L., 2007: The double-ITCZ problem in IPCC AR4 coupled GCMs: Ocean–atmosphere feedback analysis. *J. Climate*, **20**, 4497–4525, doi:10.1175/JCLI4272.1.

Liu, L. L., and R. X. Huang, 2012: The global subduction/obduction rates: Their interannual and decadal variability. *J. Climate*, **25**, 1096–1115, doi:10.1175/2011JCLI4228.1.

Liu, Z. G., S. G. H. Philander, and R. C. Pacanowski, 1994: A GCM study of tropical–subtropical upper-ocean water exchange. *J. Phys. Oceanogr.*, **24**, 2606–2623, doi:10.1175/1520-0485(1994)024<2606:AGSOTU>2.0.CO;2.

Liu, Z. Y., and B. Y. Huang, 1997: A coupled theory of tropical climatology: Warm pool, cold tongue, and Walker circulation. *J. Climate*, **10**, 1662–1679, doi:10.1175/1520-0442(1997)010<1662:ACTOTC>2.0.CO;2.

Locarnini, R. A., and Coauthors, 2013: *Temperature*. Vol. 1, *World Ocean Atlas 2013*, NOAA Atlas NESDIS 73, 40 pp. [Available online at https://data.nodc.noaa.gov/woa/WOA13/DOC/woa13_vol1.pdf.]

Luyten, J. R., J. Pedlosky, and H. Stommel, 1983: The ventilated thermocline. *J. Phys. Oceanogr.*, **13**, 292–309, doi:10.1175/1520-0485(1983)013<0292:TVT>2.0.CO;2.

Madec, G., 2008: NEMO ocean engine. Note Pôle Modélisation de l'Institut Pierre-Simon Laplace Tech. Note 27, 217 pp. [Available online at http://www.nemo-ocean.eu/content/download/5302/31828/file/NEMO_book.pdf.]

——, and M. Imbard, 1996: A global ocean mesh to overcome the North Pole singularity. *Climate Dyn.*, **12**, 381–388, doi:10.1007/BF00211684.

Manucharyan, G. E., C. M. Brierley, and A. V. Fedorov, 2011: Climate impacts of intermittent upper ocean mixing induced by tropical cyclones. *J. Geophys. Res.*, **116**, C11038, doi:10.1029/2011JC007295.

Marshall, J. C., A. J. G. Nurser, and R. G. Williams, 1993: Inferring the subduction rate and period over the North Atlantic. *J. Phys. Oceanogr.*, **23**, 1315–1329, doi:10.1175/1520-0485(1993)023<1315:ITSRAP>2.0.CO;2.

McCreary, J. P., and P. Lu, 1994: Interaction between the subtropical and equatorial ocean circulations: The subtropical cell. *J. Phys. Oceanogr.*, **24**, 466–497, doi:10.1175/1520-0485(1994)024<0466:IBTSAE>2.0.CO;2.

Mechoso, C. R., and Coauthors, 1995: The seasonal cycle over the tropical Pacific in coupled ocean–atmosphere general circulation models. *Mon. Wea. Rev.*, **123**, 2825–2838, doi:10.1175/1520-0493(1995)123<2825:TSCOTT>2.0.CO;2.

Moum, J. N., A. Perlin, J. D. Nash, and M. J. McPhaden, 2013: Seasonal sea surface cooling in the equatorial pacific cold tongue controlled by ocean mixing. *Nature*, **500**, 64–67, doi:10.1038/nature12363.

Murtugudde, R., J. Beauchamp, C. R. McClain, M. Lewis, and A. J. Busalacchi, 2002: Effects of penetrative radiation on the upper tropical ocean circulation. *J. Climate*, **15**, 470–486, doi:10.1175/1520-0442(2002)015<0470:EOPROT>2.0.CO;2.

Pan, Y. H., and A. H. Oort, 1983: Global climate variations connected with sea surface temperature anomalies in the eastern equatorial Pacific Ocean for the 1958–73 period. *Mon. Wea. Rev.*, **111**, 1244–1258, doi:10.1175/1520-0493(1983)111<1244:GCVCWS>2.0.CO;2.

Polton, J. A., and D. P. Marshall, 2003: Understanding the structure of the subtropical thermocline. *J. Phys. Oceanogr.*, **33**, 1240–1249, doi:10.1175/1520-0485(2003)033<1240:UTSOTS>2.0.CO;2.

Qin, X., A. Sen Gupta, and E. van Sebille, 2015: Variability in the origins and pathways of Pacific equatorial undercurrent water. *J. Geophys. Res. Oceans*, **120**, 3113–3128, doi:10.1002/2014JC010549.

Qiu, B., and R. X. Huang, 1995: Ventilation of the North Atlantic and North Pacific—Subduction versus obduction. *J. Phys.*

Oceanogr., **25**, 2374–2390, doi:10.1175/1520-0485(1995)025<2374:VOTNAA>2.0.CO;2.

Rayner, N. A., D. E. Parker, E. B. Horton, C. K. Folland, L. V. Alexander, D. P. Rowell, E. C. Kent, and A. Kaplan, 2003: Global analyses of sea surface temperature, sea ice, and night marine air temperature since the late nineteenth century. *J. Geophys. Res.*, **108**, 4407, doi:10.1029/2002JD002670.

Richter, I., 2015: Climate model biases in the eastern tropical oceans: Causes, impacts and ways forward. *Wiley Interdiscip. Rev.: Climate Change*, **6**, 345–358, doi:10.1002/wcc.338.

Rodgers, K. B., M. A. Cane, N. H. Naik, and D. P. Schrag, 1999: The role of the Indonesian Throughflow in equatorial Pacific thermocline ventilation. *J. Geophys. Res.*, **104**, 20 551–20 570, doi:10.1029/1998JC900094.

——, B. Blanke, G. Madec, O. Aumont, P. Ciais, and J. C. Dutay, 2003: Extratropical sources of equatorial Pacific upwelling in an OGCM. *Geophys. Res. Lett.*, **30**, 1084, doi:10.1029/2002GL016003.

Rothstein, L. M., R. H. Zhang, A. J. Busalacchi, and D. Chen, 1998: A numerical simulation of the mean water pathways in the subtropical and tropical Pacific Ocean. *J. Phys. Oceanogr.*, **28**, 322–343, doi:10.1175/1520-0485(1998)028<0322:ANSOTM>2.0.CO;2.

Samelson, R. M., and G. K. Vallis, 1997: Large-scale circulation with small diapycnal diffusion: The two-thermocline limit. *J. Mar. Res.*, **55**, 223–275, doi:10.1357/0022240973224382.

Song, X., and G. J. Zhang, 2009: Convection parameterization, tropical Pacific double ITCZ, and upper-ocean biases in the NCAR CCSM3. Part I: Climatology and atmospheric feedback. *J. Climate*, **22**, 4299–4315, doi:10.1175/2009JCLI2642.1.

Spall, M. A., 1992: Cooling spirals and recirculation in the subtropical gyre. *J. Phys. Oceanogr.*, **22**, 564–571, doi:10.1175/1520-0485(1992)022<0564:CSARIT>2.0.CO;2.

Stommel, H., 1979: Determination of water mass properties of water pumped down from the Ekman layer to the geostrophic flow below. *Proc. Natl. Acad. Sci. USA*, **76**, 3051–3055, doi:10.1073/pnas.76.7.3051.

Sun, D. Z., J. Fasullo, T. Zhang, and A. Roubicek, 2003: On the radiative and dynamical feedbacks over the equatorial Pacific cold tongue. *J. Climate*, **16**, 2425–2432, doi:10.1175/2786.1.

Takahashi, K., and D. S. Battisti, 2007: Processes controlling the mean tropical Pacific precipitation pattern. Part I: The Andes and the eastern Pacific ITCZ. *J. Climate*, **20**, 3434–3451, doi:10.1175/JCLI4198.1.

Taylor, K. E., R. J. Stouffer, and G. A. Meehl, 2012: An overview of CMIP5 and the experiment design. *Bull. Amer. Meteor. Soc.*, **93**, 485–498, doi:10.1175/BAMS-D-11-00094.1.

Thomas, M. D., 2012: Sverdrup balance and three dimensional variability of the meridional overturning circulation. Ph.D. thesis, University of East Anglia, 178 pp.

——, A.-M. Treguier, B. Blanke, J. Deshayes, and A. Voldoire, 2015: A Lagrangian method to isolate the impacts of mixed layer subduction on the meridional overturning circulation in a numerical model. *J. Climate*, **28**, 7503–7517, doi:10.1175/JCLI-D-14-00631.1.

Tiedtke, M., 1989: A comprehensive mass flux scheme for cumulus parameterization in large-scale models. *Mon. Wea. Rev.*, **117**, 1779–1800, doi:10.1175/1520-0493(1989)117<1779:ACMFSF>2.0.CO;2.

Toyama, K., A. Iwasaki, and T. Suga, 2015: Interannual variation of annual subduction rate in the North Pacific estimated from a gridded Argo product. *J. Phys. Oceanogr.*, **45**, 2276–2293, doi:10.1175/JPO-D-14-0223.1.

Tsuchiya, M., R. Lukas, R. A. Fine, E. Firing, and E. Lindstrom, 1989: Source waters of the Pacific Equatorial Undercurrent. *Prog. Oceanogr.*, **23**, 101–147, doi:10.1016/0079-6611(89)90012-8.

Valdivieso Da Costa, M., and B. Blanke, 2004: Lagrangian methods for flow climatologies and trajectory error assessment. *Ocean Modell.*, **6**, 335–358, doi:10.1016/S1463-5003(03)00023-4.

——, H. Mercier, and A. M. Treguier, 2005: Effects of the mixed layer time variability on kinematic subduction rate diagnostics. *J. Phys. Oceanogr.*, **35**, 427–443, doi:10.1175/JPO2693.1.

Vallis, G. K., 2000: Large-scale circulation and production of stratification: Effects of wind, geometry, and diffusion. *J. Phys. Oceanogr.*, **30**, 933–954, doi:10.1175/1520-0485(2000)030<0933:LSCAPO>2.0.CO;2.

Vannière, B., E. Guilyardi, T. Toniazzo, G. Madec, and S. Woolnough, 2014: A systematic approach to identify the sources of tropical SST errors in coupled models using the adjustment of initialised experiments. *Climate Dyn.*, **43**, 2261–2282, doi:10.1007/s00382-014-2051-6.

Wang, C., L. Zhang, S.-K. Lee, L. Wu, and C. R. Mechoso, 2014: A global perspective on CMIP5 climate model biases. *Nat. Climate Change*, **4**, 201–205, doi:10.1038/nclimate2118.

Warner, M. J., J. L. Bullister, D. P. Wisegarver, R. H. Gammon, and R. F. Weiss, 1996: Basin-wide distributions of chlorofluorocarbons CFC-11 and CFC-12 in the North Pacific: 1985–1989. *J. Geophys. Res.*, **101**, 20 525–20 542, doi:10.1029/96JC01849.

Williams, R. G., M. A. Spall, and J. C. Marshall, 1995: Does Stommel's mixed layer ''demon'' work? *J. Phys. Oceanogr.*, **25**, 3089–3102, doi:10.1175/1520-0485(1995)025<3089:DSMLW>2.0.CO;2.

Yin, F. L., and E. S. Sarachik, 1993: Dynamics and heat balance of steady equatorial undercurrents. *J. Phys. Oceanogr.*, **23**, 1647–1669, doi:10.1175/1520-0485(1993)023<1647:DAHBOS>2.0.CO;2.

Yu, Y., and D. Z. Sun, 2009: Response of ENSO and the mean state of the tropical Pacific to extratropical cooling and warming: A study using the IAP coupled model. *J. Climate*, **22**, 5902–5917, doi:10.1175/2009JCLI2902.1.

Zuidema, P., and Coauthors, 2016: Challenges and prospects for reducing coupled climate model SST biases in the eastern tropical Atlantic and Pacific Oceans: The U.S. CLIVAR eastern tropical oceans synthesis working group. *Bull. Amer. Meteor. Soc.*, **97**, 2305–2328, doi:10.1175/BAMS-D-15-00274.1.